metals

MDPI

Article

Wear Behavior of Nb Alloyed Gray Cast Iron for Automotive Brake Disc Application

Pietro Tonolini [1,*], Lorenzo Montesano [1], Annalisa Pola [1], Gianpietro Bontempi [2] and Marcello Gelfi [1]

[1] Department of Mechanical and Industrial Engineering, University of Brescia, Via Branze 38, 25123 Brescia, BS, Italy
[2] Fonderia di Torbole S.r.l., Via Travagliato, 18, 25030 Torbole Casaglia, BS, Italy
* Correspondence: p.tonolini002@unibs.it

Abstract: Gray cast iron (GCI) with a pearlitic matrix and type-A graphite remains the most widely used material in the manufacturing of brake discs. To reduce the environmental impact of disc wear during braking, alternative materials and/or compositions to the standard ones are being studied. In this study, the effect of variation in niobium content (0–0.7 wt%) on microstructure and wear behavior of samples machined from brake discs made of hypoeutectic gray cast iron was investigated. The wear behavior of GCI was examined through pin-on-disc (PoD) wear tests using low-metallic-friction material discs as the counterparts. Microstructural analyses and hardness measurements were also conducted to evaluate the effect of Nb addition on the morphology of graphite, eutectic cells, and distribution of carbides. In addition, the wear mechanisms of different samples were evaluated using scanning electron microscope analysis. The results revealed that adding 0.3% of Nb promotes the highest wear resistance of the alloys.

Keywords: brake discs; cast iron; niobium; wear

Citation: Tonolini, P.; Montesano, L.; Pola, A.; Bontempi, G.; Gelfi, M. Wear Behavior of Nb Alloyed Gray Cast Iron for Automotive Brake Disc Application. *Metals* **2023**, *13*, 365. https://doi.org/10.3390/met13020365

Academic Editor: Amilcar Ramalho

Received: 20 January 2023
Revised: 7 February 2023
Accepted: 9 February 2023
Published: 11 February 2023

1. Introduction

In a braking event, the pistons inside the caliper squeeze two pads against the side of the disc rim or braking band, converting the kinetic energy of a moving vehicle into thermal energy generated by friction between the mating surfaces [1]. Therefore, similar to any tribosystem, the tribological behavior of the braking system depends on the properties of both the disc and pad materials used, and is influenced by speed, braking pressure, temperature, and humidity [2].

Gray cast iron (GCI) with a pearlitic matrix and type-A graphite remains the most widely used alloy in the production of brake discs for passenger vehicles. The presence of type-A graphite flakes promotes high thermal conductivity and diffusivity of the alloy, whereas the pearlite matrix guarantees appropriate mechanical properties [3,4]. Furthermore, the excellent vibration damping, together with good castability, workability, and low cost [5,6], make GCI alloys difficult to replace for disc brake applications, especially for entry-level cars, despite their high density and low corrosion resistance [7].

However, it has been proven for years that the sliding wear process of a braking system contributes to the emission of non-exhaust traffic-related PM10 (particles with an average aerodynamic diameter D: 2.5 μm < D < 10 μm) and PM2.5 (particles with D: 0.1 μm <D < 2.5 μm) derived from the wear of both discs and pads [8], affecting human health, especially in urban areas [9]. Therefore, it is necessary to limit the pollution of the braking systems. To promote this, the proposal of the new Euro 7 regulation 2022/0365(COD) [10] sets for the first time a limit on the brake particle emissions of 7 mg/km of PM10 for vehicles until 2034, which will thereafter become stricter. The fact that the limit has been imposed only on PM10 emissions could be counterproductive, as it could lead to an increase in the emission of even finer particles, and therefore result in greater harm to human

health [11]; however, this is beyond the scope of this work. Despite this, recent studies have already demonstrated a reduction of 50% in brake system emissions by improving the wear resistance of the disc by employing heat treatment [12] or by the application of wear-resistant coatings [13–17], thus contributing to both reducing pollution and increasing the life of brake discs. In fact, for this purpose, it is nowadays possible to find commercial solutions for premium cars that involve the use of wear-resistant coatings [18,19]. Unfortunately, these solutions are too expensive for lower car segments. Therefore, it is necessary to develop cheaper alternative solutions. Among others, one almost inexpensive method to control the properties of gray cast iron consists of tailoring the microstructure through the addition of alloying elements.

Niobium is a refractory metal (Tm = 2468 ± 10 °C) that has been widely used for decades as a micro-alloyed element (<0.1%) in steels owing to the refined grain size effect during thermomechanical processing by the strain-induced precipitation of nanosized NbC or NbCN [20,21], resulting in an increase in strength [22].

However, unlike steel, cast iron does not employ Nb as frequently, and the majority of research on the addition of this element to cast iron focuses on white cast iron for applications requiring wear resistance [23–25].

Regarding gray cast iron alloys, as demonstrated in previous studies, the addition of Nb promotes the refinement of the eutectic cells (ECs) and graphite structure, as well as a reduction in the interlamellar pearlite spacing, favoring an increase in hardness and tensile strength [23,26–30]. Furthermore, the addition of Nb up to 0.2% in cast iron used for cylinder heads also improves the fatigue and thermal fatigue properties of the alloy [30–32]. However, the proposed refining mechanism, level of refinement, and corresponding increase in mechanical properties are not always comparable among different studies. Nb also affects the wear behavior of gray cast iron via the precipitation of Nb carbide into the matrix. In this regard, the use of Nb in brake discs is not new [33], even though it seems to have found renewed interest [34–36]. However, the data obtained from the literature reveal a significant scatter in the wear rate trend as a function of the Nb concentration in the alloy, and a detailed study on the involvement of NbC precipitates in the wear mechanism has never been conducted.

In this study, the wear resistance of gray cast iron samples, taken from brake discs industrially produced with different percentages of Nb, was evaluated. The tribological behavior was investigated through pin-on-disc-type laboratory tests using pad material discs as the counterparts. The wear behavior was then correlated with the microstructural features of the alloys under examination. The results of this work will be used to identify a more wear-resistant Nb composition that will then be tested on a brake inertia dynamometer equipped with a particle emission collector to evaluate PM10 emissions from a complete brake system.

2. Materials and Methods

Four brake disc batches with a fixed bell were industrially produced, as the simplest geometry achievable, following the standard foundry procedures: cupola-furnace melting, stream inoculation with ferrosilicon 75, and casting into sand molds using an in-line plant. Each batch presented different niobium contents (0%, 0.3%, 0.51%, and 0.72%), as shown in Table 1, where the mean chemical composition of the discs is shown.

Table 1. Mean chemical composition of the investigated discs (wt%).

Samples	C	Si	Mn	P	S	Cr	Mo	Sn	Ti	Nb	CE *
D-0	3.20	1.91	0.63	0.04	0.14	0.1	0.01	0.08	0.02	0.00	3.8
D-0.3	3.38	1.58	0.63	0.04	0.13	0.1	0.01	0.07	0.01	0.30	3.9
D-0.5	3.26	1.62	0.55	0.04	0.10	0.2	0.01	0.05	0.01	0.51	3.8
D-0.7	3.24	1.59	0.52	0.04	0.09	0.2	0.01	0.05	0.01	0.72	3.8

* CE (carbon equivalent) = %C + (%Si + %P)/3.

To investigate the homogeneity of the distribution of the precipitated carbides inside the braking band of discs D-0.3, D-0.5, and D-0.7, metallographic characterization was performed on two cross sections, prepared following the standard metallographic procedures. In detail, the samples were taken from each disc in two positions of the rim, that is, a position close to the gate and a position named opposite to the gate (90° to the gates) (Figure 1a). Nb carbide analysis was carried out using an optical microscope Leica DMI 5000M (Leica Microsystem, Wetzlar, Germany) equipped with image analyzer LAS 4.12 software (4.12, Leica Microsystem, Wetzlar, Germany) on 10 micrographs collected at a magnification of 500× from each position in the cross-section, that is, bottom, mold parting line, and upper position (Figure 1b), for a total of 60 micrographs for each disc. The output of the image software analysis was the average total area of the carbides (μm²) and the area of the largest carbide (μm²) detected in each position (Figure 1b) for each cross-section. The maximum area of carbide for each disc was then calculated as the average of the three largest carbides detected in each position.

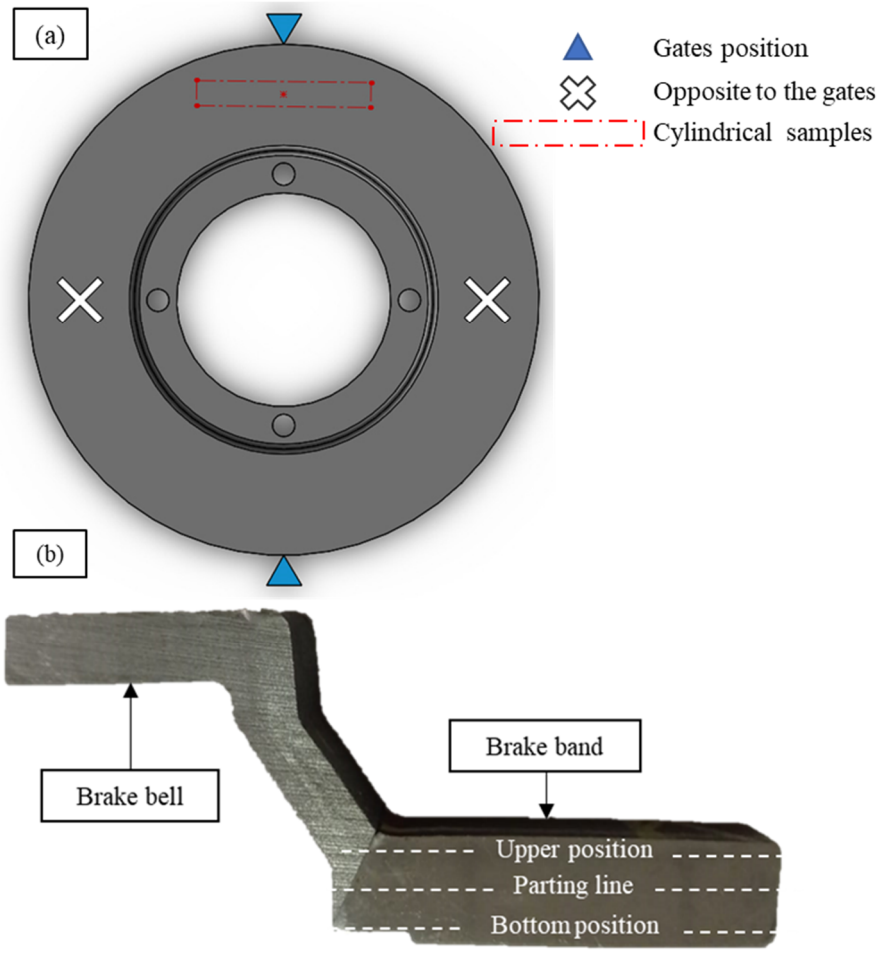

Figure 1. (**a**) Schematic drawing of the top view of a brake disc indicating the gates and the position named opposite to the gates and (**b**) Cross-section view of the considered brake discs.

Subsequently, samples for microstructural characterization were machined from the centerline of each braking band of the four brake discs and shaped into cylinders with a diameter of 10 mm and a length of 100 mm (dashed rectangle of Figure 1a). The cross-sections of the cylinders were polished to a 1 μm finishing and then analyzed.

Ten images with a magnification of 100× were collected from each sample to classify the graphite morphology according to UNI EN ISO 945-1 by using an optical microscope (Leica DMI 5000M, Leica Microsystem, Wetzlar, Germany).

The effect of Nb addition on the microstructure of the samples was investigated, after chemical etching with 2% Nital, through the same optical microscope and a scanning electron microscope (LEO EVO 40, Carl Zeiss AG, Milan, Italy) integrated with an energy-dispersive spectroscopy microprobe (EDS, Oxford Instruments, Wiesbaden, Germany). The eutectic cell densities of the different samples were evaluated using a digital microscope (Leica DMS300, Leica Microsystem, Wetzlar, Germany) after chemical etching with the Stead reagent.

The effect of Nb addition on the hardness of GCI samples was investigated through the average of five Brinell measurements (187.5 Kg and 2.5 mm carbide ball). HB 10/3000 measurements were also performed at the foundry's laboratory on the surfaces of the braking band, confirming the trend found on the machined samples' increasing Nb content. Furthermore, the possible influence of Nb addition on the mechanical properties of the pearlitic matrix was evaluated by the average value of 10 micro-Vickers indentations (300 g, Mitutoyo Hm200, Mitutoyo Italiana srl, Lainate, Italy).

To simulate the tribological behavior of brake discs [37], pin-on-disk (PoD) dry wear tests were performed at room temperature using a THT tribometer (CSM Instruments, Peseux, Switzerland). For this purpose, cylindrical pins were machined from the cylindrical samples taken from the discs, as mentioned above, with a size of Ø 4 mm × 10 mm, and then finished to obtain the roughness (Ra) of the two parallel circular surfaces of approximately 0.4 μm. The counterparts for the wear test were manufactured starting from standard commercial low-metallic copper-free [38] brake pad friction material in the form of a hot-pressed disc with a diameter of 50 mm. The average composition of the friction material is listed in Table 2.

Table 2. EDS qualitative chemical composition of the friction material, acquired on an area of about 20 mm^2.

Elements	C	O	Mg	Al	Si	S	Ca	Ti	Cr	Fe	Zn	Sn
Contents (wt%)	51.12	28.16	5.22	2.06	1.17	0.93	0.64	1.38	0.59	6.54	0.54	1.65

The test parameters were chosen to identify possible differences between the wear resistances of the samples under investigation within a reasonably limited time. In particular, a sliding speed of 1 m/s and a load of 9 N (0.71 MPa, approximately the mean nominal pressure of city traffic [16]) were applied for a total sliding distance of 15 km, with a wear track radius of 16 mm. During the tests, the friction force was monitored and the coefficient of friction (CoF) was obtained as the ratio between the friction force and the applied load, then plotted as a function of the sliding distance.

Preliminary wear tests conducted on the same pins highlighted the great variability both in the wear rates and friction coefficients as a function of the friction material disc used, underlining the strong non-homogeneity of the pad material and therefore its importance in the tribological system. For this reason, after a test evaluated as a run-in step for the friction material, the pins were tested using the same friction disc. The results presented are the average of three test repetitions for each pin. The pins were therefore tested in a random sequence, again to avoid a possible influence of the heterogeneity of the friction material also along the thickness of the disc on the results (i.e., wear rate and coefficient of friction).

The mass of the pins was measured before and after each test using an analytical balance with a precision of 10^{-4} g to estimate the mass loss during the test (Δm). The specific wear rate, K_a, was calculated for each pin as: $K_a = \frac{\Delta m}{\rho d F}$ (m^2/N), where ρ is the density of the pins (7.2 g/cm^3), d is the sliding distance, and F is the applied load.

To investigate the wear mechanisms and possible differences related to the different amounts of alloyed Nb, the surfaces of the worn pins were observed at the end of the test using a scanning electron microscope and an energy-dispersive spectroscopy microprobe.

Finally, the pin cross-sections were analyzed by SEM to further investigate the wear mechanism.

3. Results and Discussion

3.1. Microstructure

As expected, the microstructural analysis showed the presence of Nb-rich particles in all samples alloyed with the relevant amounts of Nb. As an example, Figure 2 displays the SEM backscattered images of sample D-0.3. In Figure 2a, several white particles are detectable with different shapes: elongated, rod-shaped, Y- and V-shaped, or cuboid and triangular. EDS analysis revealed that these phases were effectively niobium carbide particles (Figure 2b and Table 3), and the shape of these particles was common for all the Nb-alloyed samples. Considering the simulation calculation of NbC precipitation and the microstructural observation conducted by Zhou et al. [39], the elongated NbC particles precipitated during the solidification process, while the cuboid particles precipitated in the liquid phase as primary carbides.

The EDS analysis shown in Table 3 reveals the presence of Ti within the Nb-rich particles. As reported in Table 1, all the investigated cast irons contained at least 0.01% Ti. The presence of Ti inside the Nb-rich particles was also found in other gray cast irons with different Nb levels [32,36,39–41]. By analogy with ductile cast irons, Ti could remain as an accompanying element in NbC [42] or could be related to the fact that oxide precursors (Ti-, Si-, Mg- oxides) present in the liquid phase can act as inoculants for NbC precipitates [43].

Furthermore, it is interesting to note the presence of MnS particles (Figure 2b) in proximity to or on top of NbC particles. It is likely that these particles can act as heterogeneous nuclei for some primary MnS particles.

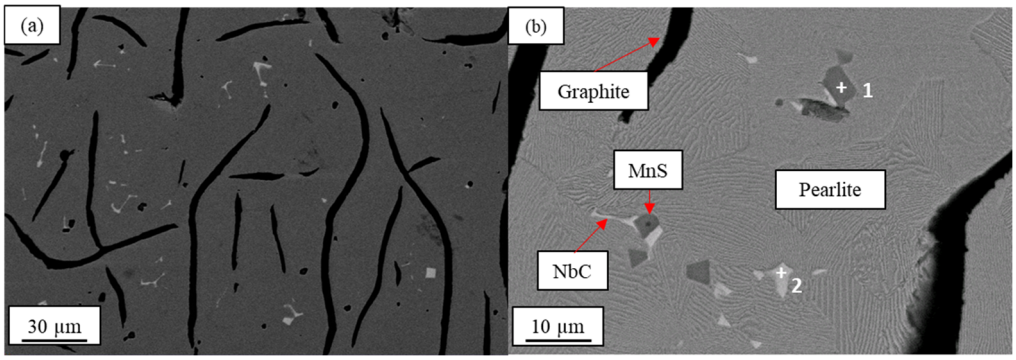

Figure 2. SEM images of D-0.3 sample. (**a**) low magnification, (**b**) high magnification, where +1 and +2 identify the location of the EDS analyses reported in Table 3.

Table 3. EDS analysis (wt%) of Figure 2b.

Spectrum	C	S	Mn	Ti	Fe	Nb
1	-	37.93	54.59	-	7.48	-
2	26.15	-	-	1.72	2.29	69.85

The homogeneous distribution of these carbides within the braking band of the brake discs was confirmed. In fact, from the histogram in Figure 3, it can be observed that both the total area of carbides and the maximum area of the largest carbides are comparable in the two investigated positions (i.e., at the gate and opposite to the gate) for each disc. Hence, the samples machined from the center of the braking band can be considered representative of the entire brake disc. Furthermore, it is evident from Figure 3 that by increasing the Nb content, the total area of the carbides as well as the area of the largest carbides increases, as also reported by other authors [26,30,39].

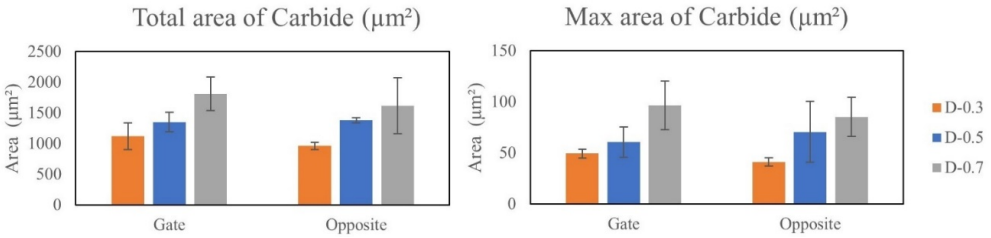

Figure 3. Carbide distribution by image analysis.

The morphology of graphite is shown in Figure 4. All samples were characterized by graphite flakes of form I, type-A, and size 4, according to the ISO945-1 standard, indicating that Nb addition does not affect the graphite morphology. Furthermore, the area fraction of graphite (%) measured in the samples accounted for 13.3%, 14.5%, 12.3%, and 10.7% for samples D-0, D-0.3, D-0.5, and D-0.7, respectively. The graphite content was related to the CE of the alloy. As can be noted from Table 1, the CE of the considered alloy slightly differs from one sample to the other because of the difficulty in obtaining a fixed chemical composition in an industrial process. Moreover, under the hypothesis that all Nb binds with C to form NbC, the resulting CE would be 3.85%, 3.88%, 3.75%, and 3.69% for samples D-0, D-0.3, D-0.5, and D-0.7, respectively. This new trend explains the trend in the graphite content.

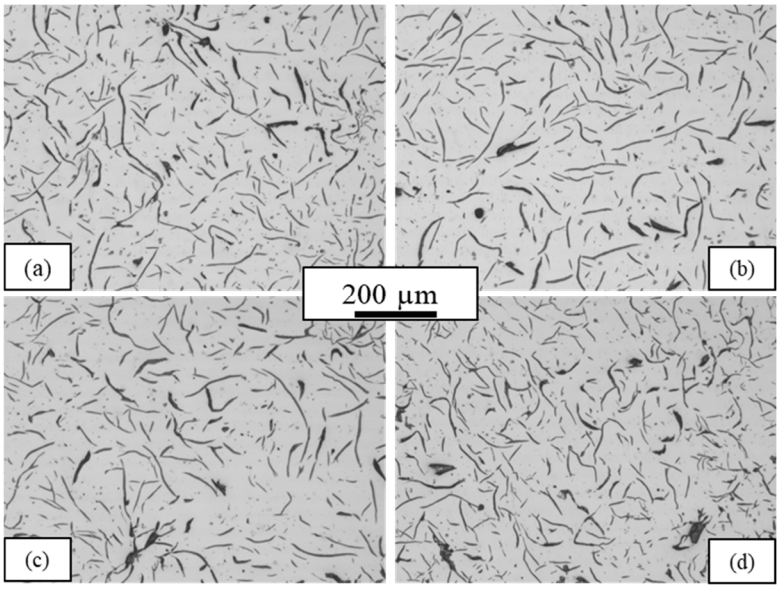

Figure 4. Graphite morphologies of the samples (**a**) D-0; (**b**) D-0.3; (**c**) D-0.5 and (**d**) D-0.7.

In Figure 5, the results of the graphite quantification by image analysis of 10 micrographs are presented. Figure 5a shows the average length of the 10 longest graphite flakes of type-A. The addition of Nb seems to promote refinement of the graphite, whose average length is shorter than that of the D-0 sample by 11%, 12%, and 18% for samples D-0.3, D-0.5, and D-0.7, respectively. Therefore, refinement appeared to be effective for the lowest concentrations of Nb. Similar results were also found in other studies [32,44], with a reduction in the graphite length of 11% for the addition of Nb up to 0.2 (wt%), while other authors reported a graphite length reduction of 56% for 0.27% Nb [39]. Furthermore, considering the graph in Figure 5b, the number of graphite flakes that account for size classes 3 and 4 according to ISO945-1 appears to decrease as the Nb content increases.

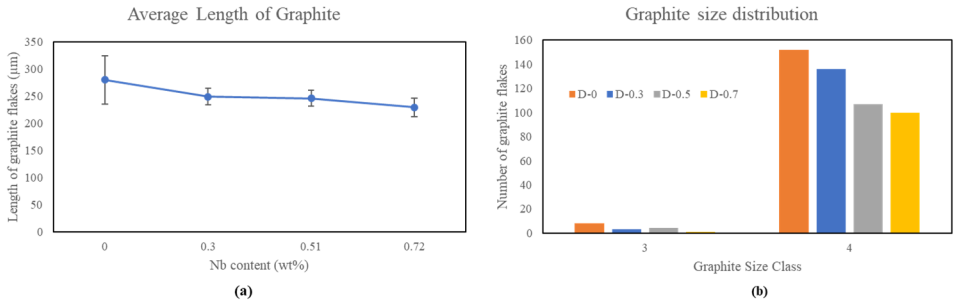

Figure 5. (**a**) Average length of graphite and (**b**) graphite size distribution.

As shown in Figure 6 and Table 4, small MnS and NbC particles are detected within the graphite flakes. It is well accepted that complex (Mn, X)S particles (usually <5 µm) act as heterogeneous nucleation sites for graphite during eutectic reaction [45]. Similarly, graphite refinement encountered for samples D-0.3, D-0.5, and D-0.7 could be caused by the graphite nucleating effect of small primary NbC particles precipitated before the eutectic temperature [32,36]. The higher the number of nucleation sites, the higher the nucleation rate; thus, the refinement of the graphite flakes is promoted. Furthermore, Nb prevents carbon from moving during solidification, which limits its ability to grow and causes it to become thin and short [26,28].

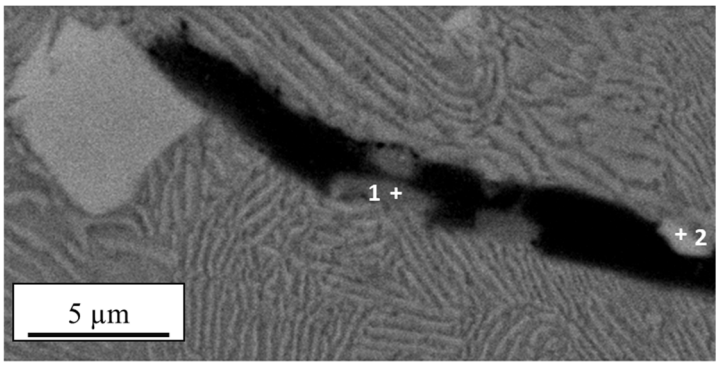

Figure 6. BS SEM image of the sample D-0.3 where +1 and +2 identify the location of the EDS analyses reported in Table 4.

Table 4. EDS analyses (wt%) of Figure 6.

Spectrum	C	O	Mg	Si	S	Ti	V	Mn	Fe	Nb
1	N/A	-	-	-	30.99	-	-	45.23	23.78	-
2	N/A	12.46	1.04	1.08	-	1.02	1.09	-	14.47	68.83

According to the optical microscope images in Figure 7, the microstructure of each sample after Nital 2% etching is characterized by a fully pearlitic matrix. Some NbC particles with different shapes and sizes were also visible within the microstructure of the Nb alloyed samples (Figure 7b–d).

Although the pearlite lamellar spacing and pearlite grain size were not statistically evaluated in this work, according to the literature, the addition of Nb up to 0.8% promotes pearlite refinement. In fact, according to some authors [28,39,41], Nb in solid solution in austenite decreases the eutectoid temperature and increases the nucleation rate and, on the other hand, Nb precipitates prevent carbon migration favoring a further pearlite refinement. A reduction in the pearlite interlamellar spacing should promote an increase in pearlite strength, which corresponds to an increase in hardness [46]. However, only a few authors [30,41,44] have conducted micro-HV measurements on pearlite colonies, and they concluded that Nb addition to GCI does not affect the pearlite hardness values. Similar

results were also presented in this study. This means that Nb is not a strong perlitizer element, especially if other strong perlitizers such as Sn are present in the alloy.

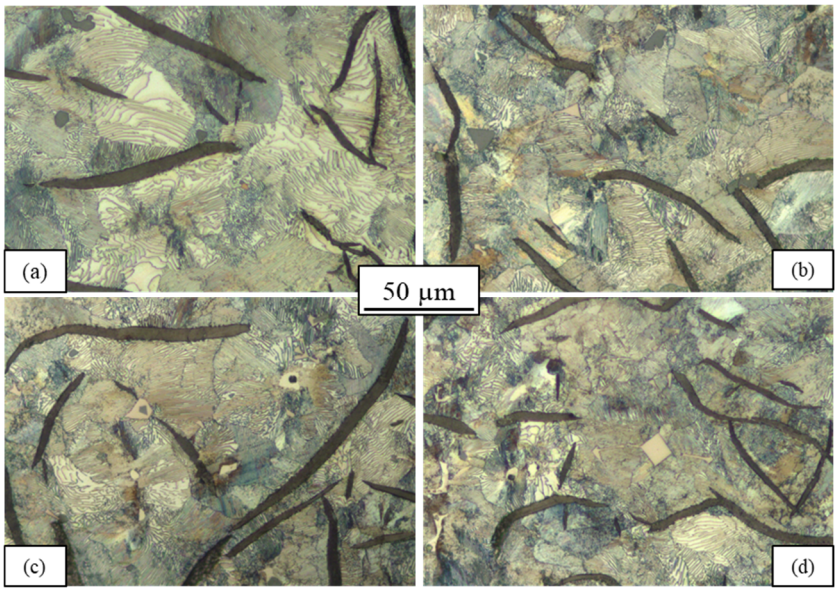

Figure 7. Microstructure of samples (**a**) D-0; (**b**) D-0.3; (**c**) D-0.5, and (**d**) D-0.7.

The microstructure presented in Figure 8 highlights the contours of the eutectic cells for different samples etched using Stead's reagent. It should be noted that the addition of Nb promotes refinement of the ECs; even if the addition is higher than 0.3%, the effect is attenuated. In fact, the measured EC densities were 26%, 22%, and 28% higher for samples D-0.3, D-0.5, and D-0.7 compared with D-0.

In the hypoeutectic GCI and Nb quantities considered in this work, NbC particles are already available in the liquid when primary austenite begins to form [36,39]. According to the literature works [45–47], particles of Nb(C, N) observed inside austenite dendrites would promote the nucleation of these, refining them, and therefore indirectly would also increase the number of eutectic cells. However, owing to the quasi-eutectic composition of the alloy under investigation, only a few austenite dendrites formed at the eutectic temperature. ECs represent eutectic solidification units that are formed as a result of the cooperative growth of graphite and austenite during the eutectic reaction. Graphite is the leading phase during the eutectic reaction; thus, some graphite nuclei will form inside the eutectic liquid, and their growth will produce as many eutectic cells as the graphite nuclei [47]. In this scenario, the refinement of the eutectic cell size seems to be a direct consequence of the increased graphite nucleation rate following the addition of Nb, which results in a higher number of graphite cores that are shorter and thinner, from which a higher number of eutectic cells are generated, as also supported by other authors [27,28,33]. Furthermore, as for the refinement of graphite length, also the increased ECs density is related to an enhancement in the mechanical properties of the alloy [48,49].

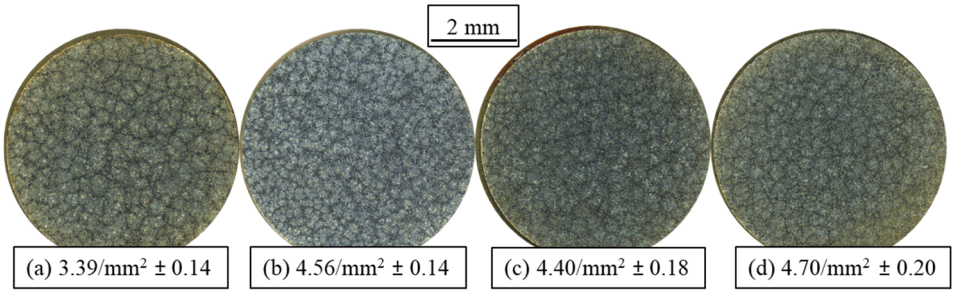

Figure 8. Eutectic cell density of samples (**a**) D-0; (**b**) D-0.3; (**c**) D-0.5, and (**d**) D-0.7.

3.2. Hardness Measurements

As shown in Figure 9a, the average Brinell hardness values increased slightly with increasing Nb content. This increase is probably due to the refinement of ECs together with the homogeneous dispersion of hard NbC primary precipitates, with a fraction area that increases with Nb content, as shown in Figure 3. Similar results were also found in other studies [28,34], where the hardness increment was related to perlite refinement, together with the presence of NbC particles. However, in the present case, the micro-Vickers hardness measurements performed on the pearlitic matrix of the samples, as shown in Figure 9b, do not suggest a clear pearlite refinement effect following the addition of Nb. This is probably due to the presence of strong perlitizer elements (i.e., Sn) already in the base alloy.

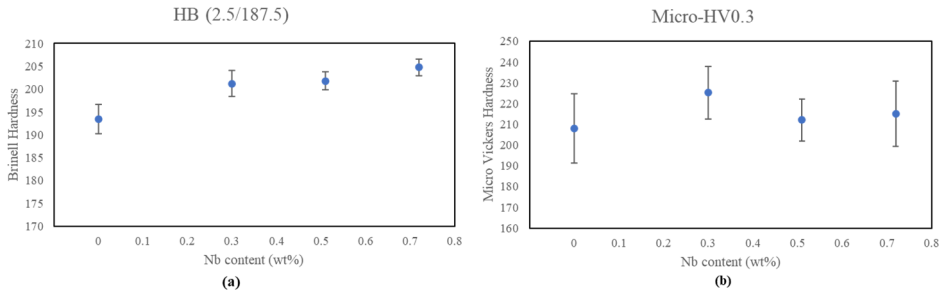

Figure 9. Effect of Nb addition on the hardness (**a**) Brinell and (**b**) micro-Vickers.

3.3. Tribological Behavior

Figure 10a shows a representative trend of the coefficient of friction (CoF) for each sample with the sliding distance recorded during the PoD test. In all the cases, the CoF reached a steady-state condition after approximately 1500 m of sliding. The steady-state CoF differs slightly between the samples, as shown in Figure 10b. However, it must be noted that the measured CoF values are in the range of typical values reported in the literature for the combination of cast iron discs and low-metallic Cu-free pads [50].

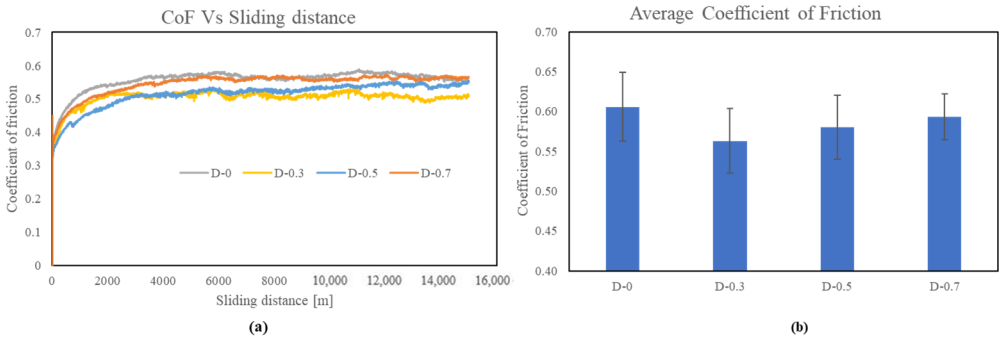

Figure 10. Coefficient of friction: (**a**) representative trend Vs sliding distance; (**b**) samples average values.

Regarding the specific wear rate, Figure 11 shows that the most wear-resistant composition is the one with the lowest Nb alloying content among those tested (i.e., D-0.3), whose wear rate is 27.8% lower than that registered for the D-0 sample. With a further increase in the Nb content, the wear resistance of the alloys decreased slightly, as the wear rates of the D-0.5 and D-0.7 samples were 23.1% and 21.7% lower than that of the D-0 sample, respectively.

In general, the wear resistance enhancement of samples D-0.3, D-0.5, and D-0.7 concerning sample D-0 could be ascribed to the increase in hardness following alloying with Nb (Figure 9a). It is well known that the increase in hardness is related to an increase in the plastic deformation resistance, promoting a higher wear resistance of the alloy [2]. However, in this case, the slight increase in the wear rate with increasing Nb addition was neither reflected in the hardness measurements shown in Figure 8a, nor in the micro-HV trend of Figure 8b. Furthermore, the hard NbC particles can act as initial friction surfaces, thus behaving as load-bearing phases [28], and promoting a general wear resistance enhancement of alloys D-0.3, D-0.5, and D-0.7 compared with D-0.

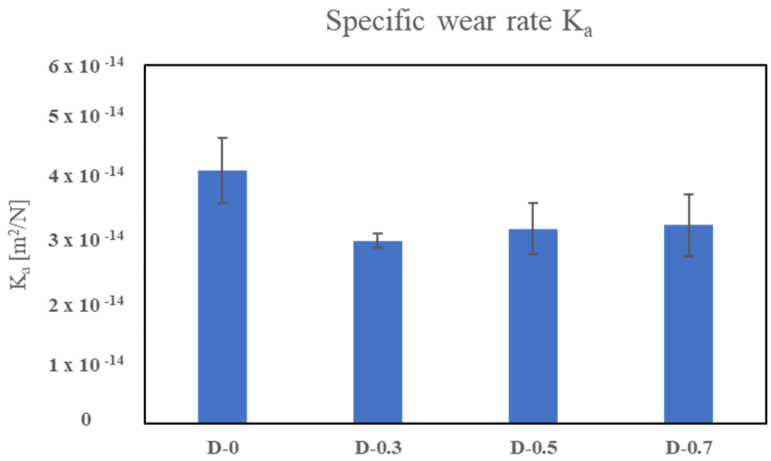

Figure 11. Specific wear rate Ka.

To further analyze the tribological behavior, the morphologies of the worn surfaces of all tested pins are presented in the SEM images in Figure 12, whereas the cross-sections of the worn pins are shown in Figure 13. The abrasive wear mechanism seems to be predominant under all investigated conditions, as indicated by the presence of abrasive grooves (Figure 12). These plow grooves can be generated by the sliding of the hard particles embedded in the friction material disc (two-body abrasive wear), as well as by the presence of oxidized debris between the mating surfaces (three-body abrasive wear). In fact, the presence of friction material debris on the surfaces of the pins is demonstrated, as highlighted by the white arrows in Figures 12 and 13, and by the EDS analyses of Table 5, where Mg and Sn elements from the pad were detected, suggesting that adhesive wear also occurs to some extent. However, some of these wear fragments seemed to be placed inside the craters on the surfaces of the pins, probably because some coarse graphite flakes peeled off during sliding [34].

Furthermore, some NbC particles were identified on the worn surfaces, as can be observed from the backscatter images in Figure 12b,c. The magnification of the detail presented in Figure 12b suggests that some NbC particles are effective in stopping some groove advancement, whereas other particles can be passed by the scratches without severe deformation, as shown in Figure 12c.

However, the coarser particles of NbC, especially if oriented unfavorably in the sliding direction, that is, with the edges protruding from the surface, as shown in Figure 13d, can experience brittle fracture owing to their poor toughness, generating hard debris that can promote an increase in three-body abrasive wear [23]. Considering that the size of these particles increased as the Nb content increased, this phenomenon could contribute to the slight increase in the wear rate of samples D-0.5 and D-0.7 with respect to sample D-0.3, notwithstanding the increase in the overall hardness of the samples.

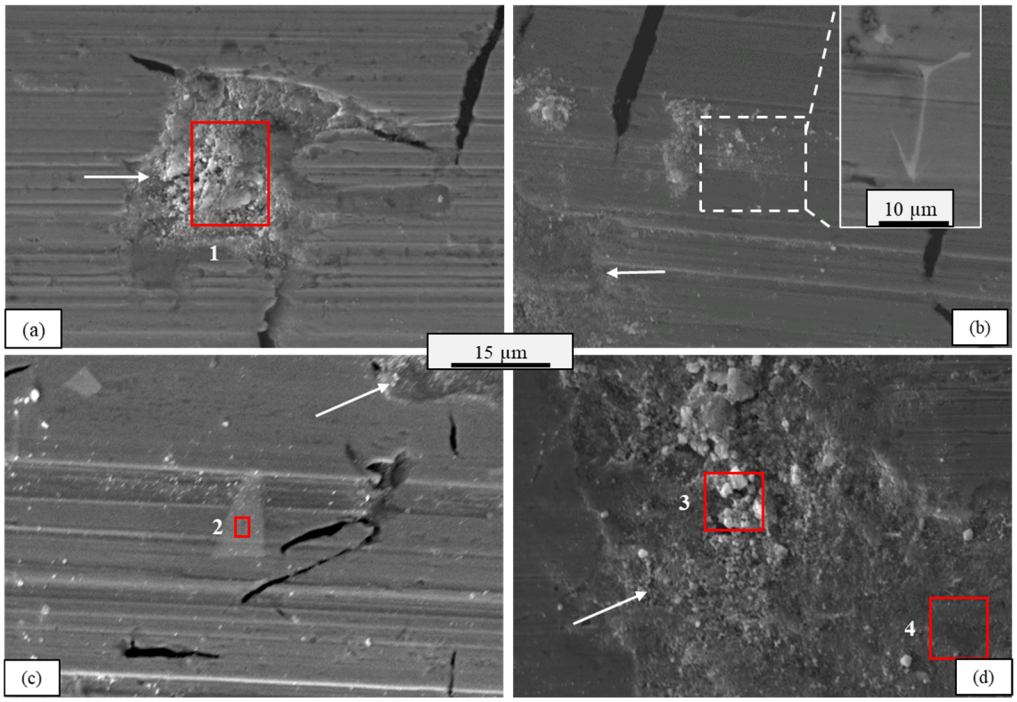

Figure 12. Worn surfaces of the pins (**a**) D-0; (**b**) D-0.3; (**c**) D-0.5; and (**d**) D-0.7. White arrows highlight pad material debris. The red rectangles (1, 2, 3 and 4) identify the location of the EDS analyses reported in Table 5. The white dashed square in figure 12b identify the area where it was detected the NbC particle shown at higher magnification in the white rectangle.

Table 5. EDS analysis (wt%) of Figure 12.

Spectrum	C	O	Mg	Al	Si	S	Mn	Ti	Fe	Sn	Nb
1	N/A	33.02	1.60	-	1.65	0.71	0.77	-	62.25	-	-
2	N/A	-	-	-	-	-	-	1.85	2.96	-	95.19
3	N/A	44.26	1.93	0.84	1.16	0.73	-	-	49.26	1.82	-
4	N/A	46.16	1.41	0.93	1.21	-	-	-	48.34	1.96	-

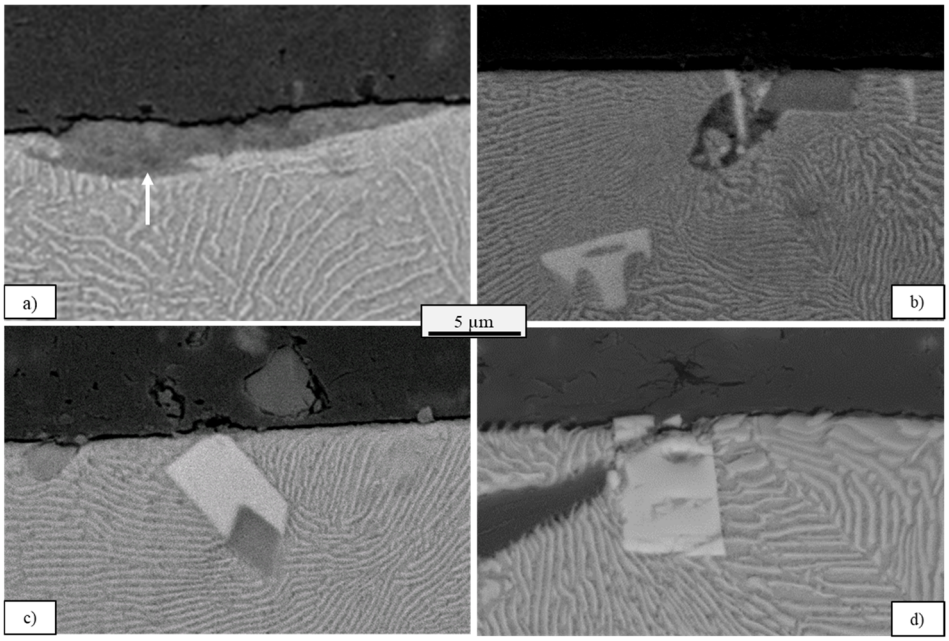

Figure 13. Cross-sectional view of the worn pins (**a**) D-0; (**b**) D-0.3; (**c**) D-0.5; and (**d**) D-0.7. White arrow in (**a**) highlight pad material debris.

4. Conclusions

In this study, the effect of different niobium additions (0%, 0.30%, 0.51%, 0.72%) on the microstructure and wear behavior of samples machined from brake-disc hypoeutectic gray cast iron was investigated. The wear behavior of GCI was examined by PoD wear tests performed with low-metallic friction material discs as counterparts. The presence of NbC particles in the microstructure of all samples alloyed with Nb was verified by using an optical microscope. NbC particles, having both cuboid and elongated shapes, appeared evenly distributed within the braking band of the cast iron samples, and their quantity and size increased with the addition of Nb.

Microstructural analysis revealed a pearlitic matrix for all the considered samples, indicating that, in the presence of other strong perlitizer elements, the addition of Nb did not affect the microstructure, as also confirmed by the micro-HV measurements performed in the matrix. Additionally, the graphite shape was unaffected by Nb, while the graphite flake length was slightly reduced, probably because the formation of small NbC particles in the liquid acted as heterogeneous nuclei for the graphite, enhancing their nucleation rate. This graphite refinement was also associated with a reduction in eutectic cell size. The reduced graphite flake length and the refinement of eutectic cells, together with the presence of well-distributed carbide particles, were responsible for the increase in hardness measured on the Nb-added samples as compared to the base alloy.

Abrasive wear was detected as the main wear mechanism in the PoD tests, even if some adhesive wear also occurred. Compared with the base alloy, the addition of Nb improved the wear strength, favored by the increase in hardness and the presence of hard NbC particles that could act as a load-bearing phase. However, the highest wear resistance was recorded for relatively low Nb addition (i.e., 0.3% Nb). Further addition of Nb did not appreciably modify the cast iron properties and negatively induced the coarsening of NbC particles. During sliding, coarse particles with poor toughness can easier experience brittle fracture, generating hard debris that promotes an increase in the three-body abrasive wear. Hence, it is advisable to not exceed 0.3% Nb in the composition of cast iron to improve their wear resistance and maintain low alloying costs.

Author Contributions: Conceptualization, G.B., A.P. and P.T.; methodology, P.T. and L.M.; investigation, P.T., L.M. and M.G.; writing—original draft preparation, P.T.; writing—review and editing, A.P. and M.G.; supervision, A.P. and M.G.; project administration, G.B.; funding acquisition, G.B. All authors have read and agreed to the published version of the manuscript.

Funding: This research was funded by the Ministry of Economic Development, EcoBrakeSystem (EBS) project, call FRI n° F/150040/01/X40, CUP B38I20000280005

Data Availability Statement: Not applicable.

Acknowledgments: Authors would like to acknowledge Elkem ASA Foundry Products, Norway, for the support in the preparation of the samples.

Conflicts of Interest: The authors declare no conflict of interest

References

1. Andrews, D. *Braking of Road Vehicles*, 1st ed. ed. Butterworth-Heinemann, 2014.
2. Straffelini, G. *Friction and Wear (Springer Tracts in Mechanical Engineering)*; Springer: Cham, Switzerland, 2015.
3. Jimbo, Y.; Mibe, T.; Akiyama, K.; Matsui, H.; Yoshida, M.; Ozawa, A. Development of high thermal conductivity cast iron for brake disk rotors. In *SAE Transactions*; SAE International: Warrendale, PA, USA,1990. https://doi.org/10.4271/900002.
4. Xu, W.; Ferry, M.; Wang, Y. Influence of alloying elements on as-cast microstructure and strength of gray iron. *Mater. Sci. Eng. A* **2005**, *33*, 326–333. https://doi.org/10.1016/j.msea.2004.08.030.
5. Maluf, O.; Angeloni, M.; Milan, M.; Spinelli, D.; Wladimir, W.; Filho, B. Development of materials for automotive disc brakes. *Pesqui. Technol Minerva* **2004**, *2,* 149-158.
6. Grabiec, T. Wear and Friction Behavior of Friction Pairs Tested with Different Types of Grey Cast Iron and Low Met Friction Material. *SAE Int. J. Passeng. Cars—Mech. Syst.* **2014**, *7*, 1361–1368. https://doi.org/10.4271/2014-01-2525.
7. Djafri, M.; Bouchetara, M.; Busch, C.; Weber, S. Effects of humidity and corrosion on the tribological behaviour of the brake disc materials. *Wear* **2014**, *321*, 8–15. https://doi.org/10.1016/j.wear.2014.09.006.

8. Grigoratos T.; Martini G. Non-exhaust traffic related emission. Brake and tyre wear PM. In *European Commission Joint Research Centre- Institute of Energy and Transport 2014*; Publications Office of the European Union: Luxembourg, 2014. Available online: https://ec.europa.eu/jrc/en/publication/eur-scientific-and-technical-research-reports/non-exhaust-traffic-related-emissions-brake-and-tyre-wear-pm (accessed on 20 July 2020).
9. Gonet, T.; Maher, B.A. Airborne, Vehicle-Derived Fe-Bearing Nanoparticles in the Urban Environment: A Review. *Environ. Sci. Technol.* **2019**, *17*, 9970–9991. https://doi.org/10.1021/acs.est.9b01505.
10. *2022/0365(COD)*; Type-Approval of Motor Vehicles and Engines and of Systems, Components and Separate Technical Units Intended for such Vehicles, with Respect to Their Emissions and Battery Durability (Euro 7). European Parliament Legislative Observatory: Strasbourg, France, 2022.
11. Puisney, C.; Oikonomou, E.K.; Nowak, S.; Chevillot, A.; Casale, S.; Baeza-Squiban, A.; Berret, J.-F. Brake wear (nano)particle characterization and toxicity on airway epithelial cells: In vitro. *Environ. Sci. Nano* **2018**, *5*, 1036–1044. https://doi.org/10.1039/c7en00825b.
12. Perricone, G.; Matějka, V.; Alemani, M.; Valota, G.; Bonfanti, A.; Ciotti, A.; Olofsson, U.; Söderberg, A.; Wahlström, J.; Nosko, O.; et al. A concept for reducing PM10 emissions for car brakes by 50%. *Wear* **2018**, *396–397*, 135–145. https://doi.org/10.1016/j.wear.2017.06.018.
13. Aranke, O.; Algenaid, W.; Awe, S.; Joshi, S. Coatings for Automotive Gray Cast Iron Brake Discs: A Review. *Coatings* **2019**, *9*, 552. https://doi.org/10.3390/coatings9090552.
14. Federici, M.; Menapace, C.; Moscatelli, A.; Gialanella, S.; Straffelini, G. Pin-on-disc study of a friction material dry sliding against HVOF coated discs at room temperature and 300 degrees C. *Tribol. Int.* **2017**, *115*, 89–99. https://doi.org/10.1016/j.triboint.2017.05.030.
15. Menapace, C.; Mancini, A.; Federici, M.; Straffelini, G.; Gialanella, S. Characterization of airborne wear debris produced by brake pads pressed against HVOF-coated discs. *Friction* **2019**, *8*, 421–432. https://doi.org/10.1007/s40544-019-0284-4.
16. Wahlström, J.; Lyu, Y.; Matjeka, V.; Söderberg, A. A pin–on–disc tribometer study of disc brake contact pairs with respect to wear and airborne particle emissions. *Wear* **2017**, *384–385*, 124–130. https://doi.org/10.1016/j.wear.2017.05.011.
17. Tonolini, P.; Montesano, L.; Pola, A.; Landriani, E.; Gelfi, M. The effect of laser-cladding on the wear behavior of gray cast iron brake disc. *Procedia Struct. Integr.* **2021**, *33*, 1152–1161. https://doi.org/10.1016/j.prostr.2021.10.129.
18. Elbrigmann, T. Hard like Diamond. *Porsche Cust. Mag. Christophorus* **2017**, *4*, 384.
19. Bosch. iDisc. Available online: https://www.bosch-mobility-solutions.com/en/solutions/driving-safety/idisc/ (accessed on 01 March 2020).
20. Dutta, B.; Palmiere, E.; Sellars, C. Modelling the kinetics of strain induced precipitation in Nb microalloyed steels. *Acta Mater.* **2001**, *49*, 785–794. https://doi.org/10.1016/S1359-6454(00)00389-X.
21. DeArdo, A.J. Niobium in modern steels. *Int. Mater. Rev.* **2003**, *48*, 371–402. https://doi.org/10.1179/095066003225008833.
22. Sun, L.-Y.; Liu, X.; Xu, X.; Lei, S.-W.; Li, H.-G.; Zhai, Q.-J. Review on niobium application in microalloyed steel. *J. Iron Steel Res. Int.* **2022**, *29*, 1513–1525. https://doi.org/10.1007/s42243-022-00789-1.
23. Bedolla-Jacuinde, A. Niobium in Cast Irons. In *Progress in Metallic Alloys*; Vadim, G., Ed.; IntechOpen: Rijeka, Croatia, 2016. https://doi.org/10.5772/64498.
24. Pourasiabi, H.; Gates, J. Effects of niobium macro-additions to high chromium white cast iron on microstructure, hardness and abrasive wear behaviour. *Mater. Des.* **2021**, *212*, 110261. https://doi.org/10.1016/j.matdes.2021.110261.
25. Filipovic, M.; Kamberovic, Z.; Korac, M.; Gavrilovski, M. Microstructure and mechanical properties of Fe–Cr–C–Nb white cast irons. *Mater. Des.* **2013**, *47*, 41–48. https://doi.org/10.1016/j.matdes.2012.12.034.
26. Zhou, W.; Zhu, H.; Zheng, D.; Hua, Q.; Zhai, Q. Effect of niobium on solidification structure of gray cast iron. *TMS Annu. Meet.* **2010**, *3*, 817–828.
27. Wenbin, Z.; Hongbo, Z.; Dengke, Z.; Hongxing, Z.; Qin, H.; Qijie, Z. Niobium alloying effect in high carbon equivalent grey cast iron. *China Foundry* **2011**, *8*, 36–40.
28. Mohrbacher, H.; Zhai, Q. Niobium alloying in grey cast iron for vehicle brake discs. In *Materials Science and Technology Conference and Exhibition 2011, MS&T'11*; Columbus, Ohio, USA, 16–20 October 2011; Taylor & Francis: Oxford, UK; volume 1, pp. 434–445.
29. Hanna, I. Mechanical Properties of Niobium Alloyed Gray Iron. Master Thesis, Royal Institute of Technology, Stockholm Sweden, 2011.
30. Yao, Y. The Influence of Niobium Content and Cooling Rate on Mechanical Properties of Grey Cast Iron. Master Thesis, KTH Royal Institute of Technology, Stockholm, Sweden, 2019. Available online: http://urn.kb.se/resolve?urn=urn:nbn:se:kth:diva-244999 (accessed on 15 December 2022).
31. James, J.; Ronald, C.; Leonard, M.; Michael, M.; John, E. High Strength Gray Cast Iron Containing Niobium. *Patent Appl. WO 2008/105987 A1,* **2008**.
32. Pan, S.; Zeng, F.; Su, N.; Xian, Z. The effect of niobium addition on the microstructure and properties of cast iron used in cylinder head. *J. Mater. Res. Technol.* **2019**, *9*, 1509–1518. https://doi.org/10.1016/j.jmrt.2019.11.076.
33. Joachim, P.; Lotz, W. Optimized Gray Cast Iron Plate Alloy for Utility Vehicle Brake Disks. Patent Number US005894010A, 1999.
34. Li, Q.; Zhang, Y.; Zhang, Y.; Liu, H.; Ren, H.; Zhong, Y.; Huang, X.; Huang, W. Influence of Sn and Nb additions on the microstructure and wear characteristics of a gray cast iron. *Appl. Phys. A* **2020**, *126*, 282. https://doi.org/10.1007/s00339-020-03468-8.

35. Leal, G.; Enloe, C.M.; Meira, M.; Franca, E.; Nascimento, F.; Halonen, A. Wear evaluation of niobium-added cast iron for brake disc and drum applications. *SAE Int. J. Adv. Curr. Prac. Mobil.* **2020**, *3*, 980–987. https://doi.org/10.4271/2020-01-1627.
36. Weitao, S.; Bin, W.; Xiaoliang, L.; Yuqian, W.; Jian, Z. Controlling the tribology performance of gray cast iron by tailoring the microstructure. *Tribol. Int.* **2022**, *167*, 107343. https://doi.org/10.1016/j.triboint.2021.107343.
37. Metinoz, I.; Matejka, V.; Alemani, M.; Wahlström, J.; Perricone, G. Could pin-on-disc tribometers be used to study the friction/wear performance of disc brake materials? In Proceedings of the Eurobrake, Milano, Italy, 13–15 June 2016.
38. Chan, D.; Stachowiak, G.W. Review of automotive brake friction materials. *Proc. Inst. Mech. Eng. Part D: J. Automob. Eng.* **2004**, *218*, 953–966. https://doi.org/10.1243/0954407041856773.
39. Zhou, Z.-H.; Song, S.-Q.; Cromarty, R.; Chen, Y.-L.; Xue, Z.-L. The Precipitation of Niobium Carbide and Its Influence on the Structure of HT250 for Automobile Wheel Hubs. *Materials* **2021**, *14*, 6109. https://doi.org/10.3390/ma14206109.
40. Devecili, A.O.; Yakut, R. The Effect of Nb Supplement on Material Characteristics of Iron with Lamellar Graphite. *Adv. Mater. Sci. Eng.* **2014**, *2014*, 465947. https://doi.org/10.1155/2014/465947.
41. Reis, B.C.M.; dos Santos, A.J.; Pereira, N.F.S.; do Carmo, D.J.; de Faria, G.L.; Câmara, M.A.; de Faria, P.E.; Abrão, A.M. Effect of Nb Addition on the Machinability of a Pearlitic Gray Cast Iron. *J. Mater. Eng. Perform.* **2022**, *31*, 5983–5999. https://doi.org/10.1007/s11665-022-06669-9.
42. Ahmed, M.; Soliman, M.; Youssef, M.; Bähr, R.; Nofal, A. Effect of Niobium on the Microstructure and Mechanical Properties of Alloyed Ductile Irons and Austempered Ductile Irons. *Metals* **2021**, *11*, 703. https://doi.org/10.3390/met11050703.
43. Chen, X.; Zhao, L.; Zhang, W.; Mohrbacher, H.; Wang, W.; Guo, A.; Zhai, Q. Effects of niobium alloying on microstructure, toughness and wear resistance of austempered ductile iron. *Mater. Sci. Eng. A* **2019**, *760*, 186–194. https://doi.org/10.1016/j.msea.2019.05.100.
44. Hasbrouck, M. THE EFFECTS OF MOLYBDENUM, CHROMIUM, AND NIOBIUM ON GRAY IRON FOR BRAKE ROTOR APPLICATIONS. Master Thesis, Michigan Technological University, Houghton, MI, USA, 2021.
45. Riposan, I.; Chisamera, M.; Stan, S.; Hartung, C.; White, D. Three-stage model for nucleation of graphite in grey cast iron. *Mater. Sci. Technol.* **2010**, *26*, 1439–1447. https://doi.org/10.1179/026708309X12495548508626.
46. Clayton, P.; Danks, D. Effect of interlamellar spacing on the wear resistance of eutectoid steels under rolling-sliding conditions. *Wear* **1990**, *135*, 369–389. https://doi.org/10.1016/0043-1648(90)90037-B.
47. Pero-Sanz Elorz, J.A.; Fernández González, D.; Verdeja, L.F.; (Eds.). Stable Eutectic—Graphite Morphologies. In *Physical Metallurgy of Cast Irons*; Springer International Publishing: Cham, Switzerland, 2018; pp. 19–31.
48. Collini, L.; Nicoletto, G.; Konečná, R. Microstructure and mechanical properties of pearlitic gray cast iron. *Mater. Sci. Eng. A* **2008**, *488*, 529–539. https://doi.org/10.1016/j.msea.2007.11.070.
49. Willidal, T.; Bauer, W.; Schumacher, P. Stress/strain behaviour and fatigue limit of grey cast iron. *Mater. Sci. Eng. A* **2005**, *413-414*, 578–582. https://doi.org/10.1016/j.msea.2005.08.200.
50. Lyu, Y.; Leonardi, M.; Wahlström, J.; Gialanella, S.; Olofsson, U. Friction, wear and airborne particle emission from Cu-free brake materials. *Tribol. Int.* **2019**, *141*, 105959. https://doi.org/10.1016/j.triboint.2019.105959.